Extending the collocation method to multidimensional molecular dynamics: Direct determination of the intermolecular potential of Ar-H sub 2 O from tunable far-infrared laser spectr...

ARTICLE *in* THE JOURNAL OF PHYSICAL CHEMISTRY · OCTOBER 1990

Impact Factor: 2.78 · DOI: 10.1021/j100383a044

2 AUTHORS:

Ronald C. Cohen

394 PUBLICATIONS **8,684** CITATIONS

SEE PROFILE

Richard J Saykally

University of California, Berkeley

460 PUBLICATIONS **28,045** CITATIONS

SEE PROFILE

on nonannealed Ni/TiO_2 surfaces. On the annealed Ni/TiO_2 surface, adsorption of N_2 is associative as well as dissociative at 80 K, whereas CO adsorption is completely dissociative.[10] On an Ni/Al_2O_3 surface, however, N_2 is adsorbed molecularly at 80 K, just as CO.[11] It seems that the annealed Ni/TiO_2 surface represents the SMSI state, a conclusion that is somewhat strengthened by its similarity to a Ti-Ni alloy with regard to the adsorptive properties.

Conclusions

The following features in the N(1s) and He II spectra of adsorbed nitrogen are found to be useful in characterizing the various adsorbed species. Physical adsorption of N_2 is characterized by a single feature around ~403 eV (e.g., on the TiO_2 surface). Two types of weakly chemisorbed N_2 species are identified, one showing only a single N(1s) feature corresponding to an unscreened final state at 405 eV (e.g., on Ti and Ni-Ti alloy surfaces) and the other showing two features at 401 and 406 eV corresponding to screened and unscreened final states (e.g., on Ni, Ni/Al_2O_3, and nonannealed Ni/TiO_2 surfaces). The feature at 397 eV corresponds to the atomic species (e.g., on Ti and annealed Ni/TiO_2 surfaces). Observation of a single feature at 405 eV due to chemisorption signifies much weaker adsorption than when two features at 401 and 405 eV are found. Physisorbed N_2 shows three features in the He II spectrum around 9, 11, and 14 eV due to $3\sigma_g$, $1\pi_u$, and $2\sigma_u$ orbitals, respectively. Chemisorbed N_2 shows only two features around 8.5 and 13 eV due to $(3\sigma_g + 1\pi_u)$ and $2\sigma_u$, respectively. The atomic nitrogen shows a single feature around 5.6 eV in the He II spectrum. In Table I, we have summarized the N(1s) and valence orbital binding energies of N_2 adsorbed on the various surfaces studied by us.

The main conclusions with regard to the nature of the adsorption of N_2 on the different surfaces are as follows:

(i) Adsorption of N_2 is molecular on both Ni/Al and Ni/Al_2O_3 surfaces at 80 K.

(ii) N_2 physisorbs on TiO_2 and reduced TiO_2 surfaces at 80 K; on the latter there is also dissociation.

(iii) N_2 is adsorbed partly dissociatively on clean Ti and Ti-Ni alloy surfaces. There is also very weak chemisorption with a single N(1s) feature around 405 eV.

(iv) On a Ni/TiO_x surface, there is substantial molecular chemisorption (with two N(1s) features at 401 and 406 eV) accompanied by dissociation.

(v) Only molecular adsorption of N_2 is seen on the nonannealed Ni/TiO_2 surface just as on a Ni/Al_2O_3 surface.

(vi) On annealed Ni/TiO_2, however, we find both dissociative and molecular adsorption at 80 K (the latter desorbs at 125 K) similar to the Ni-Ti alloy surface, suggesting that the annealed Ni/TiO_2 surface may represent the SMSI state.

Acknowledgment. We thank the Department of Science and Technology, Government of India, for support of this research work.

Registry No. Ni, 7440-02-0; TiO_2, 13463-67-7; N_2, 7727-37-9.

Extending the Collocation Method to Multidimensional Molecular Dynamics: Direct Determination of the Intermolecular Potential of Ar-H_2O from Tunable Far-Infrared Laser Spectroscopy

R. C. Cohen and R. J. Saykally*

Department of Chemistry, University of California, and Material and Chemical Sciences Division, Lawrence Berkeley Laboratory, Berkeley, California 94720 *(Received: April 18, 1989)*

We present an extension of the collocation method developed by Peet and Yang (*J. Chem. Phys.* **1989**, *91*, 6598) for calculating the bound states of rotating atom-diatom systems to atom-polyatom complexes. The method is shown to be general, accurate, efficient, and straightforward to implement. The collocation algorithm is incorporated into a nonlinear least-squares program, which is used in a direct fit of far-infrared vibration-rotation spectra of the Ar-H_2O complex to a detailed analytical model for the anisotropic intermolecular potential energy surface. The surface denoted AW1 was obtained without any dynamical approximations. The minimum (D_e = 174.7 cm^{-1}, R_e = 3.598 Å) in the intermolecular potential surface occurs for the argon located in the plane of the H_2O, nearly perpendicular to the symmetry axis.

I. Introduction

A great deal of interest is currently directed toward the development of *molecular* descriptions of condensed matter behavior, and it is widely recognized that accurate intermolecular potential energy surfaces (IPS) are essential to the ultimate success of this endeavor. Despite a tremendous amount of experimental and theoretical investigation over several decades, reliable anisotropic models for intermolecular forces exist for only a few simple systems. All of these are of the form M-AB, where M denotes a rare gas atom and AB represents a linear molecular (viz, Rg-H_2,[1] Ar-HCl,[2] Ar-HF,[3] Ne-HCl,[4] and several complexes containing He[5]). The interaction between M and AB in the monomer's ground vibrational state is implicitly a two-dimensional problem, parametrized by a distance (R) and a single angle (θ).

Two serious obstacles have impeded extensions to more complex systems: (1) the lack of precise experimental probes that are sensitive to anisotropic features of the attractive wells, and (2) the lack of viable theoretical techniques for accurately describing the heavy particle dynamics that occur on complicated potential surfaces with more than two dimensions. The first of these difficulties has recently been addressed by the development of new spectroscopic approaches employing tunable infrared and far-infrared lasers and molecular beam production of weakly bound molecules. As a result many interesting multidimensional systems (e.g., Ar-H_2O,[6-8] Ar-NH_3,[9] $(HCl)_2$,[10,11] $(H_2O)_2$,[12,13] $(NH_3)_2$,[14]

(1) Leroy, R. J.; Hutson, J. M. *J. Chem. Phys.* **1987**, *86*, 837.
(2) Hutson, J. M. *J. Chem. Phys.* **1988**, *89*, 4550.
(3) Nesbitt, D. J.; Child, M. S.; Clary, D. C. *J. Chem. Phys.* **1989**, *90*, 4855.
(4) Hutson, J. M. *J. Chem. Phys.* **1988**, *91*, 4448.
(5) Danielson, L. S.; Keil, M.; Dunlop, P. J. *J. Chem. Phys.* **1988**, *88*, 4218.
(6) Cohen, R. C.; Busarow, K. L.; Laughlin, K. B.; Blake, G. A.; Havenith, M.; Lee, Y. T.; Saykally, R. J. *J. Chem. Phys.* **1988**, *89*, 4494.
(7) Cohen, R. C.; Busarow, K. L.; Lee, Y. T.; Saykally, R. J. *J. Chem. Phys.* **1990**, *92*, 167.
(8) Nesbitt, D. J. Private communication.
(9) Gwo, Dz-H.; Havenith, M.; Busarow, K. L.; Cohen, R. C.; Schmuttenmaer, C. A.; Saykally, R. J. *Mol. Phys.*, in press.

0022-3654/90/2094-7991$02.50/0

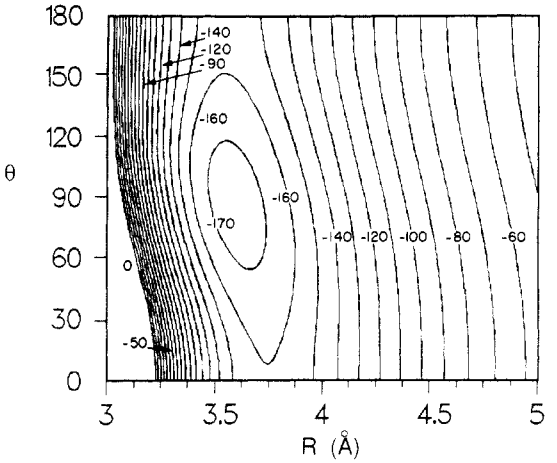

Figure 1. A cut through the AW1 potential at $\phi = 0$. This corresponds to the potential energy for motion of the argon atom in the plane of the water molecule. Contours are shown at 10-cm^{-1} intervals and contours above 0 cm^{-1} are not shown.

and CH_4–H_2O[15]) have now been investigated at a level of detail permitting an extensive characterization of the associated IPS.

The extraction of accurate potential energy surfaces from these newly acquired data is currently hampered by computational difficulties associated with the accurate calculation of the vibration–rotation energies in weakly bonded systems. The large amplitude of the vibrational motions and the strong couplings among the various degrees of freedom that are inherent in most weakly bound systems render familiar techniques for reducing multidimensional problems to a set of one-dimensional problems inoperable. It is thus essential to treat these systems with methods which are explicitly multidimensional. The rapid evolution of modern computers has made brute force variational approaches viable for calculations on multidimensional systems,[16] but such methods become prohibitively expensive for actually fitting data to a model IPS, principally because of the need for numerical evaluation of multidimensional integrals. The close-coupling method has been the most frequently used approach for this process,[1,2,4] but it is complicated and difficult to generalize. Two newly developed computational techniques hold considerable promise for extension to multidimensional problems. These are the collocation method as applied by Peet and Yang[17-21] and the discrete variable representation formalism (DVR) of Light and co-workers.[22-24] These methods combine the accuracy of basis set methods for treating the kinetic energy operator with the simplicity of representing the potential energy by its value on a grid of points in space. They both offer the advantage that no integrals need to be evaluated over the multidimensional potential energy surface, and they are easily constructed to explicitly include the effects of overall rotation of the complex. The collocation method is intrinsically the simpler of the two to implement. It offers the additional advantage that it is easier to incorporate a

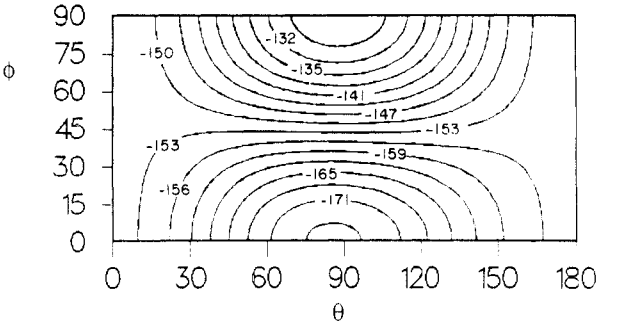

Figure 2. Anisotropy in the potential in the region of the minimum. This cut is at R = 3.6 Å. Contours are shown at 3-cm^{-1} intervals.

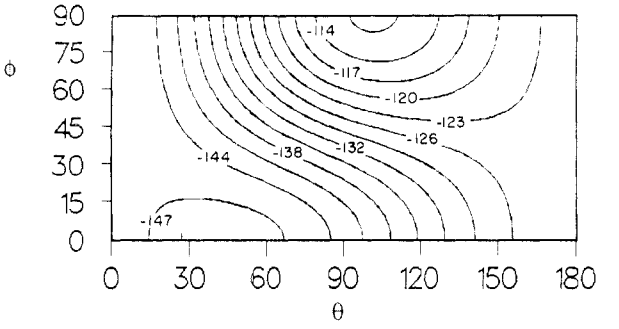

Figure 3. Anisotropy in the potential at R = 4.0 Å. Contours are shown at 3-cm^{-1} intervals.

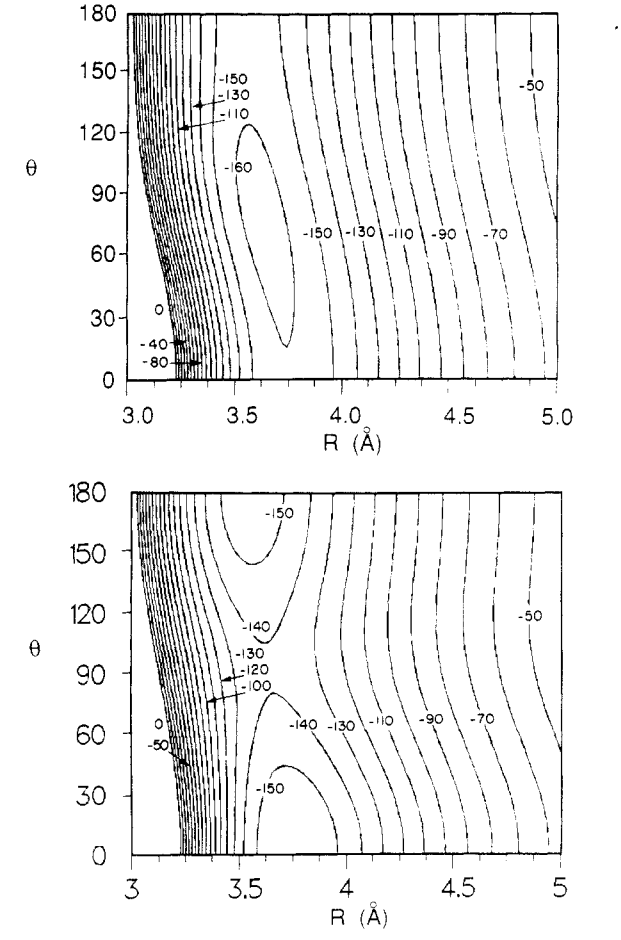

Figure 4. Transition from single to double minimum in the θ coordinate with increasing ϕ. (a, top) A cut through the potential at $\phi = 30°$. (b, bottom) A cut through the potential at $\phi = 60°$. Contours are shown at 10-cm^{-1} intervals.

(10) Blake, G. A.; Busarow, K. L.; Cohen, R. C.; Laughlin, K. B.; Lee, Y. T.; Saykally, R. J., *J. Chem. Phys.* **1988**, *89*, 6577. Blake, G. A.; Bumgarner, R. E. *J. Chem. Phys.* **1989**, *91*, 7300.
(11) Schuder, M. D.; Nelson, Jr., D. D.; Lovejoy, C. M.; Nesbitt, D. J. *J. Chem. Phys.*, in press.
(12) Busarow, K. L.; Blake, G. A.; Laughlin, K. B.; Cohen, R. C.; Lee, Y. T.; Saykally, R. J. *J. Chem. Phys.* **1988**, *89*, 1268.
(13) Huang, Z. S.; Miller, R. E. *J. Chem. Phys.* **1989**, *91*, 6613.
(14) Havenith, M.; Cohen, R. C.; Busarow, K. L.; Gwo, Dz-H.; Saykally, R. J. Manuscript in preparation.
(15) Busarow, K. L.; Cohen, R. C.; Schmuttenmaer, C. A.; Lee, Y. T.; Saykally, R. J. Manuscript in preparation.
(16) Brocks, G. *J. Chem. Phys.* **1988**, *88*, 578. Clary, D. C.; Lovejoy, C. M.; O'Neil, S. V.; Nesbitt, D. J. *Phys. Rev. Lett.* **1988**, *61*, 1576.
(17) Yang, W.; Peet, A. C. *Chem. Phys. Lett.* **1988**, *153*, 98.
(18) Peet, A. C.; Yang, W. *J. Chem. Phys.* **1989**, *90*, 1746.
(19) Peet, A. C.; Yang, W. *J. Chem. Phys.* **1989**, *91*, 6598.
(20) Yang, W.; Peet, A. C.; Miller, W. H. *J. Chem. Phys.* **1989**, *91*, 7537.
(21) Yang, W.; Peet, A. C. *J. Chem. Phys.* **1990**, *92*, 522.
(22) Bacic, Z.; Light, J. C. *J. Chem. Phys.* **1987**, *86*, 3065. Bacic, Z.; Light, J. C. *J. Chem. Phys.* **1988**, *89*, 947.
(23) Choi, S. E.; Light, J. C. *J. Chem. Phys.* **1990**, *91*, 2129.
(24) Bacic, Z.; Light, J. C. *Annu. Rev. Phys. Chem.* **1989**, *40*, 469.

nondirect product trial basis set.

In this paper we describe the extension of the collocation approach developed by Peet and Yang to a three-dimensional system, (R, θ, ϕ), the Ar–H_2O complex. We first present the application of the collocation method to atom–polyatom systems in general, and then specialize to the symmetry appropriate for Ar–H_2O and investigate the convergence of the method for this system. The formalism we describe is shown to be sufficiently accurate and efficient to warrant its use in the determination of a new anisotropic IPS for Ar–H_2O by direct fit to experimental data. The resulting potential, denoted AW1, is shown in Figures 1–4 As we have discussed previously,[6,7] Ar–H_2O is of fundamental interest because it is a prototypical three-dimensional system, and as such is a natural vehicle for the extension of methods previously applied to atom–diatom systems, and because it is one of the simplest systems which is capable of manifesting the effects of the "hydrophobic interactions".[25] Hutson has previously considered the many-body dynamics of this complex on an anisotropic IPS within the "reversed adiabatic" approximation, which specifically neglects the effects of the radial potential and any angular–radial coupling.[26] We make no such approximations here. Our theoretical accuracy is limited only by finite basis set effects, and convergence of the bound-state energies to 0.001 cm^{-1} is demonstrated. Previous investigations[27,28] of the Ar–H_2O IPS have made use of experimental data that contain information only about the average of the IPS over the angular anisotropy.

Our studies of the vibration–rotation spectrum of the Ar–H_2O cluster using tunable far-infrared laser spectroscopy have facilitated two preliminary determinations of the anisotropy in the intermolecular potential. In ref 7 we determined the effective radial IPS for three different intermolecular vibrational states. These were determined by a least-squares fit to the experimentally measured rotational term values for each level. We found significant anisotropy in the potential, as evidenced by the variation in the binding energy, which ranged from D_e = 153 to 98 cm^{-1} for the states considered. In an accompanying paper,[26] Hutson considered the anisotropy in the potential at a fixed radial position. This approximation neglects coupling between the angular and radial degrees of freedom but is expected to give a reasonable qualitative description of the anisotropy if the angular–radial coupling is small. Using the two vibrational frequencies reported in our initial study of Ar–H_2O,[6] Hutson determined a range of values for three correlated terms that describe the anisotropy of the intermolecular potential. The anisotropic terms for the IPS recommended by Hutson prove to be very good estimates of those which we determine rigorously from the full three-dimensional surface. In the present work we determine the IPS of Ar–H_2O directly and without any approximations in the dynamics.

We begin with a general description of the collocation treatment of atom–polyatom systems (section II). In section III, we describe the construction and parametrization of a trial intermolecular potential surface. We then present the results of a nonlinear least-squares fit of the experimental data collected by Cohen et al.[6,7] to this IPS (section IV). In the final section, we discuss the properties of the potential and assess the validity of approximations employed in other treatments of the dynamics.

II. Adaptation of the Collocation Method to Three-Dimensional Systems

(a) The Collocation Equations for a General Atom–Asymmetric Top Complex. The collocation method is a simple and efficient method for numerical evaluation of the bound-state eigenvalues and eigenvectors of the Schrödinger equation. In applications of this method to one-dimensional[17] (Morse oscillator) and two-dimensional[18,19] (Ar–HCl) problems, Peet and Yang have demonstrated the rapid convergence and ease of implementation

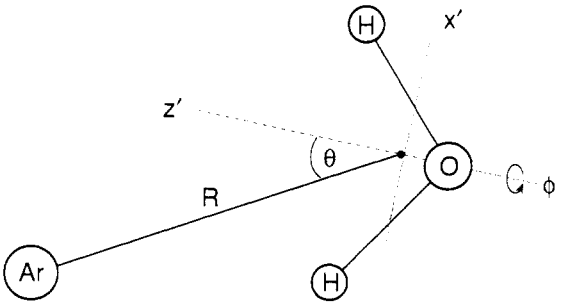

Figure 5. The coordinate system used to describe the interaction of argon with H_2O.

of the method. In essence, the collocation method amounts to an n-point quadrature approximation to the Rayleigh–Ritz variational method for solving the Schrödinger equation. The procedure for applying the collocation method is to expand the wave function as a linear combination of n basis functions. This wave function is then taken to be an exact solution to the Schrödinger equation at each of n points in the configuration space of the problem. The resulting n coupled equations then appear in the form of a generalized unsymmetric eigenvalue problem

$$[\mathbf{H} - E\Psi]\mathbf{c} = 0 \tag{1}$$

where $\mathbf{H}$ is a matrix with elements H_{ji} given by $\mathcal{H}|\Psi_i\rangle$ evaluated at the set of points $(R_j, \theta_j, \phi_j, ...)$, and Ψ is a matrix with the column vectors $|\Psi_i\rangle$, evaluated at the same set of points. The label i ranges from 1 to n, the number of basis functions in the trial wave function. The label j spans the same range but identifies the point in configuration space at which the matrix element has been evaluated. Standard eigenvalue subroutines are used to solve the matrix problem, returning E, the eigenvalues, and $\mathbf{c}$, the matrix of eigenvectors.

In extending the collocation method to atom–polyatom systems, we exploit the work of Brocks et al.,[29] who developed a general Hamiltonian describing the dynamics of two weakly bound polyatomic molecules, as well as that of Brocks and Huygen[30] and Hutson,[26] who have specifically treated the case of an atom–polyatom system. The implementation of the numerical procedures follows closely that of Peet and Yang.[17–19] We choose a generalized Jacobi coordinate system for the atom–polyatom complex; R, the vector from the center of mass of the molecule to the atom, is embedded as the pseudodiatomic z axis of a body-fixed frame for the cluster; α and β are the polar angles of R with respect to the space-fixed axis system, and θ, ϕ, and γ are the Euler angles that orient the monomer in the body-fixed frame. The choice of coordinate systems and their effects on the Hamiltonian for weakly bonded dimers is discussed in detail by Brocks et al.[29,30] They clearly demonstrate that the form of the Hamiltonian strongly depends on the particular choice of coordinates, and specifically, on the method of embedding the polyatomic monomer within the body-fixed coordinate system.[31] The internal axes may be defined such that the orientation of R in a Cartesian (x', y', z') frame with axes along the principal inertial axes of the polyatomic monomer specified by the two angles, θ and ϕ.[30] It is then possible to perform a simple integration to eliminate the angle γ. It is advantageous to associate z' with a symmetry axis of the monomer in order to exploit symmetry in the problem. For example, in the case of an atom bound to H_2O, we choose a Cartesian frame with the z' axis along the b axis of water, and associate x' with the a axis, in the plane of the monomer, Figure 5.

(25) Swope, W.; Andersen, H. C. *J. Phys. Chem.* **1984**, *88*, 6548. Watanabe, K.; Andersen, H. C. *J. Phys. Chem.* **1986**, *90*, 795.
(26) Hutson, J. M. *J. Chem. Phys.* **1990**, *92*, 157.
(27) Bickes, Jr., R. W.; Duquette, G.; van den Meijdenberg, C. J. N.; Rulis, A. M.; Scoles, G.; Smith, K. M. *J. Phys. B* **1975**, *8*, 3034.
(28) Brooks, R.; Kalos, F.; Grosser, A. E. *Mol. Phys.* **1975**, *27*, 1071.
(29) Brocks, G.; van der Avoird, A.; Sutcliffe, B. T.; Tennyson, J. *Mol. Phys.* **1983**, *50*, 1025.
(30) Brocks, G.; Huygen, T. *J. Chem. Phys.* **1986**, *85*, 4311.
(31) Although it might seem more natural to transform the coordinate system used above to one in which a third Euler angle (γ) orients the body-fixed axes with respect to the space-fixed axes and only two angles are used to orient the monomer with respect to the body fixed axes (so-called two-angle embedding), Brocks and co-workers demonstrate (ref 29) that the three-angle embedding used in the coordinate system employed above leads to a Hamiltonian which is much more convenient.

The Hamiltonian for this system, with the monomer structure fixed at the vibrationally averaged geometry, may be written as

$$\mathcal{H} = \frac{-\hbar^2}{2\mu R}\frac{\partial^2}{\partial R^2}R + \frac{\hbar^2}{2\mu R^2}(\hat{J}^2 + \hat{j}^2 - 2\hat{j}\cdot\hat{J}) + \mathcal{H}_{\text{monomer}} + V(R,\theta,\phi) \quad (2)$$

where μ is the pseudodiatomic reduced mass, $\hat{J}$ is the total angular momentum of the system, $\hat{j}$ is the internal angular momentum of the monomer, and $V(R,\theta,\phi)$ is the intermolecular potential, which is taken to be averaged over the small-amplitude vibrational motion of the monomer. We take $\mathcal{H}_{\text{monomer}}$ to be

$$H = B_x\hat{j}_x^{m^2} + B_y\hat{j}_y^{m^2} + B_z\hat{j}_z^{m^2} \quad (3)$$

The superscript m denotes angular momentum operators written in the Cartesian frame of the monomer. All other angular momentum operators are expressed in the body-fixed frame of the inertial axes of the complex.

The wave function of this system is expanded in terms of a product of angular and radial functions:

$$\Psi^J(\alpha,\beta,R,\theta,\phi,\gamma) = \frac{1}{R}\sum_{\xi=0}^{1}\sum_{\epsilon=0}^{1}\sum_{\Omega=\epsilon}^{J}\sum_{j=\Omega}^{N^\theta}\sum_{k=0}^{N^\phi}\sum_{i=1}^{N^R}C_{\xi\epsilon\Omega jki}\chi_i(R)(1 + \delta_{0\Omega})^{-1/2}\{D^{J*}_{M\Omega}(\alpha,\beta,0)S^{j\xi*}_{\Omega k}(\gamma,\theta,\phi) + (-1)^\epsilon[D^{J*}_{M-\Omega}(\alpha,\beta,0)S^{j\xi*}_{-\Omega k}(\gamma,\theta,\phi)]\} \quad (4)$$

$$S^{j\xi*}_{\Omega k}(\gamma,\theta,\phi) = (1 + \delta_{0k})^{-1/2}[D^{j*}_{\Omega k}(\gamma,\theta,\phi) + (-1)^\xi D^{j*}_{\Omega -k}(\gamma,\theta,\phi)]$$

$$\chi_i(R) = \left[\frac{2A}{\pi}\right]^{1/4}\exp[-A(R - R_i)^2]; \quad A = \frac{c^2}{(R_1 - R_2)^2}$$

Here N^θ and N^ϕ determine the size of the basis set in the angular coordinates; they are functions of (ξ,ϵ,Ω) and (ξ,ϵ,Ω,j), respectively. N^R determines the size of the radial basis. The $D^J_{M\Omega}(\alpha,\beta,\gamma)$ functions are normalized Wigner D matrices in the phase convention of Condon and Shortley. The form of the Gaussian basis in R follows the prescription Hamilton and Light[32] and has been used throughout the work of Yang and Peet.[17-19] The constant A in the Gaussians in apprropriate for equally spaced functions. We take the constant c, which determines the width of the Gaussians, to be 0.5, which proved to be satisfactory in the work of Yang and Peet.

The product of angular momentum operators is expanded as

$$-2\hat{j}\cdot\hat{J} = -2\hat{j}_z\hat{J}_z - \hat{j}_+\hat{J}_+ - \hat{j}_-\hat{J}_-$$

where

$$\hat{J}_\pm = \hat{J}_x \mp i\hat{J}_y \quad \text{and} \quad \hat{j}_\pm = \hat{j}_x \pm i\hat{j}_y$$

and $\mathcal{H}_{\text{monomer}}$ as

$$\mathcal{H} = \frac{1}{2}(B_x + B_y)\hat{j}^{m^2} + \left(B_z - \frac{1}{2}(B_x + B_y)\right)\hat{j}_z^{m^2} + \frac{1}{4}(B_x - B_y)(\hat{j}_+^{m^2} + \hat{j}_-^{m^2})$$

These operators have the following effects on the rotation matrices:

$$\hat{J}^2D^{J*}_{M,\Omega}(\alpha,\beta,0) = J(J+1)D^{J*}_{M,\Omega}(\alpha,\beta,0)$$

$$\hat{j}^{m^2}D^{j*}_{\Omega,k}(\gamma,\theta,\phi) = j(j+1)D^{j*}_{\Omega,k}(\gamma,\theta,\phi)$$

$$\hat{J}_\pm D^{J*}_{M,\Omega}(\alpha,\beta,0) = C^\pm_{J,\Omega}D^{J*}_{M,\Omega\pm1}(\alpha,\beta,0)$$

$$\hat{j}_z^{m^2}D^{jk}_{\Omega,k}(\gamma,\theta,\phi) = k^2D^{j*}_{\Omega,k}(\gamma,\theta,\phi)$$

$$\hat{j}_\pm D^{\theta*}_{\Omega,k}(\gamma,\theta,\phi) = C^\pm_{j,\Omega}D^{j*}_{\Omega\pm1,k}(\gamma,\theta,\phi)$$

$$\hat{j}_\pm^{m^2}D^{j*}_{\Omega,k}(\gamma,\theta,\phi) = F^\pm_{j,k}D^{j*}_{\Omega,k\pm2}(\gamma,\theta,\phi)$$

$$\hat{j}^2D^{j*}_{\Omega,k}(\gamma,\theta,\phi) = j(j+1)D^{j*}_{\Omega,k}(\gamma,\theta,\phi)$$

$$C^\pm_{j,\Omega} = [j(j+1) - \Omega(\Omega \pm 1)]^{1/2}$$

$$F^\pm_{j,k} = [j(j+1) - k(k \pm 1)]^{1/2}[j(j+1) - (k \pm 1)(k \pm 2)]^{1/2}$$

(32) Hamilton, I. P.; Light, J. C. *J. Chem. Phys.* **1986**, *84*, 306.

The next steps follow closely those taken by Peet and Yang in their application of the collocation method to the rotating Ar–HCl complex.[19] We act on the product wavefunction with the Hamiltonian, then multiply on the left by

$$R(1 + \delta_{0\Omega'})^{-1/2}[D^{J}_{M,\Omega'}(\alpha,\beta,0)e^{i\Omega'\gamma} + (-1)^{(\epsilon'+\Omega')}D^{J}_{M,-\Omega'}(\alpha,\beta,0)e^{-i\Omega'\gamma}], \quad (5)$$

which is an eigenfunction of the parity operator, and then integrate over α, β, and γ. This gives the set of coupled differential equations:

$$\sum_{\xi=0}^{1}\sum_{\epsilon=0}^{1}\sum_{\Omega=\epsilon}^{J}\sum_{j=\Omega}^{N^\theta}\sum_{k=0}^{N^\phi}\sum_{i=1}^{N^R}C_{\xi\epsilon\Omega jki}\left\{\left\{-\frac{\hbar}{2\mu}\chi_i''(R) + \left[\frac{\hbar^2[J(J+1) + j(j+1) - 2\Omega^2]}{2\mu R^2} + \frac{1}{2}(B_x + B_y)j(j+1) + \left[B_z - \frac{1}{2}(B_x + B_y)\right]k^2 + V(R,\theta,\phi) - E\right]\chi_i(R)\right\} \times (S^{j\xi*}_{\Omega,k}(0,\theta,\phi) + (-1)^{\epsilon+\epsilon'+\Omega}S^{j\xi*}_{\Omega,k}(0,\theta,\phi))\delta_{\Omega,\Omega'} + \left\{\frac{1}{4}(B_x - B_y)(1 + \delta_{0k})^{-1/2}[F_{jk}{}^+(S^{j\xi*}_{\Omega,k+2}(0,\theta,\phi) + (-1)^{\epsilon+\epsilon'+\Omega}S^{j\xi*}_{\Omega,k+2}(0,\theta,\phi)) + \omega_{0,k-2}F_{jk}{}^-(S^{j\xi*}_{\Omega,k-2}(0,\theta,\phi) + (-1)^{\epsilon+\epsilon'+\Omega}S^{j\xi*}_{\Omega,k-2}(0,\theta,\phi))]\chi_i(R)\right\}\delta_{\Omega,\Omega'} - \frac{\hbar^2}{2\mu R^2}[C_{J\Omega}{}^+C_{j\Omega}{}^+(S^{j\xi*}_{\Omega+1,k}(0,\theta,\phi) + (-1)^{\epsilon+\epsilon'+\Omega+1}S^{j\xi*}_{-(\Omega+1),k}(0,\theta,\phi))\delta_{\Omega',\Omega+1}\omega_{0\Omega} + C_{J\Omega}{}^-C_{j\Omega}{}^-(S^{j\xi*}_{\Omega-1,k}(0,\theta,\phi) + (-1)^{\epsilon+\epsilon'+\Omega-1}S^{j\xi*}_{-(\Omega-1),k}(0,\theta,\phi))\delta_{\Omega,\Omega-1}\omega_{0,\Omega'}]\chi_i(R)\right\} = 0 \quad (6)$$

Here $\chi_i''(R)$ indicates the second derivative of the Gaussian with respect to R and $\omega_{0M} = (1 + \delta_{0M})^{1/2}$. These equations are block diagonal in J, and noninteracting blocks may be solved separately.

The next step in the application of the collocation method requires selecting a set of n collocation points, one corresponding to each basis function. Peet and Yang demonstrated that choosing the centers of the Gaussians leads to rapid convergence in the radial coordinate. They also showed that Gauss–Legendre points of the same order as the number of angular basis functions provide a good set of points for both the Legendre $[P_j(\cos\theta)]$ and associated Legendre, $[P_j^\Omega(\cos\theta)]$ polynomials. Our tests show these to be adequate for the Wigner rotation matrices as well. The choice of points in the ϕ coordinate is discussed below, with specific reference to Ar–H_2O. Before proceeding, it is also necessary to specify a method for basis set trunctation, that is, for the functional forms of $N^\theta(\xi,\epsilon,\Omega)$ and $N^\phi(\xi,\epsilon,\Omega,j)$. The optimum choice depends on the demands of the problem in question, in particular, on the size of the anisotropic forces, the degree of symmetry present, the number of intermolecular vibrational states for which convergence is desired, and the range of J and Ω which are of interest. Peet and Yang[19] have discussed two possible choices for truncation of the basis in the θ coordinate in their study of the two-dimensional Ar–HCl complex: (1) $N^\theta = j_{\max} - \Omega + 1$, which reduces the size of the angular basis at high Ω and gives adequate convergence for some of the internal rotor levels of low j, Ω; and (2) $N^\theta = j_{\max} + 1$, which gives a basis set of constant size as Ω increases and is necessary to give adequate convergence of high j and Ω levels. Similar considerations are applicable to the three-dimensional atom–polyatom complex; the basis may be truncated to optimize the speed with which eigenvalues corresponding to low j, k, Ω internal rotor levels are converged, or it may be optimized for a more accurate characterization of all levels. We discuss below the choices we have found to be optimum, with specific reference

TABLE I: Symmetries of the Components of the Trial Wave Function for Ar–H_2O in the C_{2v} Group

symmetry	J	k	$\epsilon + \xi$
A_1	even	even	even
A_2	even	even	odd
B_1	even	odd	even
B_2	even	odd	odd
A_2	odd	even	even
A_1	odd	even	odd
B_2	odd	odd	even
B_1	odd	odd	odd

to application of the collocation method for the evaluation of the eigenvalues of Ar–H_2O.

Next, the coupled equations are forced to be exact at the set of points $[R_{i'}, \theta_{\xi'\epsilon'\Omega'j'}, \phi_{\xi'\epsilon'\Omega'j'k'}]$, which casts the coupled equations in the form of a generalized complex unsymmetrical eigenvalue problem:

$$[\mathbf{H}^J - E^J\Psi^J]\mathbf{c}^J = 0$$

$$H^J_{\xi'\epsilon'\Omega'j'k'i',\xi\epsilon\Omega jki} = \left\{-\frac{\hbar}{2\mu}\chi_i''(R_{i'}) + \left[\frac{\hbar^2[J(J+1)+j(j+1)-2\Omega^2]}{2\mu R_{i'}^2} + \frac{1}{2}(B_x + B_y)j(j+1) + \left[B_z - \frac{1}{2}(B_x+B_y)\right]k^2 + V(R_{i'},\theta_{\xi'\epsilon'\Omega'j'},\phi_{\xi'\epsilon'\Omega'j'k'})\right]\chi_i(R_{i'})\right\}Q^{jk\xi\epsilon}_{\Omega,k}[\xi'\epsilon'\Omega'j'k']\delta_{\Omega,\Omega'} + \frac{1}{4}(B_x - B_y)(1+\delta_{0k})^{-1/2}\{F_{jk}{}^{+}Q^{jk\xi\epsilon}_{\Omega,k+2}[\xi'\epsilon'\Omega'j'k'] + F_{jk}{}^{-}Q^{jk\xi\epsilon}_{\Omega,k-2}[\xi'\epsilon'\Omega'j'k']\omega_{0,(k-2)}\}\chi_i(R_{i'})\delta_{\Omega,\Omega'} - \frac{\hbar^2}{2\mu R_{i'}^2}\{C_{J\Omega}{}^{+}C_{j\Omega}{}^{+}Q^{jk\xi\epsilon}_{\Omega+1,k}[\xi'\epsilon'\Omega'j'k']\delta_{\Omega',\Omega+1}\omega_{0\Omega} + C_{J\Omega}{}^{-}C_{j\Omega}{}^{-}Q^{jk\xi\epsilon}_{\Omega-1,k}[\xi'\epsilon'\Omega'j'k']\delta_{\Omega',\Omega-1}\omega_{0\Omega'}\}\chi_i(R_{i'}) \quad (7)$$

$$Q^{jk\xi\epsilon}_{\Omega,k}[\xi'\epsilon'\Omega'j'k'] = S^{jk\xi\epsilon}_{\Omega,k}(0,\theta_{\xi'\epsilon'\Omega'j'},\phi_{\xi'\epsilon'\Omega'j'k'}) + (-1)^{\epsilon+\epsilon'+\Omega'}S^{jk\xi\epsilon}_{-\Omega,k}(0,\theta_{\xi'\epsilon'\Omega'j'},\phi_{\xi'\epsilon'\Omega'j'k'})$$

$$\Psi^J_{\epsilon'\Omega'j'k'\xi\mu i',\epsilon\Omega jk\xi i} = \chi_i(R_i)Q^{jk\xi\epsilon}_{\Omega,k}[\xi'\epsilon'\Omega'j'k']\delta_{\Omega,\Omega'} \quad (8)$$

One then solves the coupled equations by standard matrix diagonalization methods. Note that because the matrix is intrinsically unsymmetric, the eigenvalues may, in principle, be complex and the eigenvectors produced are not necessarily orthogonal. Moreover, spurious eigenvalues can appear,[17] although none have been observed during the course of this work.

(b) Symmetry Considerations and Specialization to Ar–H_2O. The formulation of the collocation method, as described in the preceding section, is general for dimeric complexes containing a rare gas atom and any polyatomic monomer. For molecules possessing symmetry, it is advantageous to reformulate the problem such that it is diagonal in both J and Γ, where Γ refers to an irreducible representation of the appropriate molecular symmetry group. The product wave function used then has the same overall form as that of eq 4, but we need to include only those functions which are of symmetry Γ. For example, in Ar–H_2O, basis functions with k = even are of A_1 or A_2 symmetry in the C_{2v} group, which is isomorphic with the molecular symmetry group for this complex. These do not mix with the k = odd functions, which are of B_1 or B_2 symmetry. In Table I, we identify those functions which transform as irreducible representations of the group C_{2v}. For an atom bound to a C_{2v} molecule, a 4-fold reduction in matrix size is achieved by employing these symmetrized basis functions. Again, the coupled equations are forced to be exact on a grid of points $[R_{i'}, \theta_{\xi'\epsilon'\Omega'j'}, \phi_{\xi'\epsilon'\Omega'j'k'}]$. Since the reduction in basis set size comes about because of symmetry in the ϕ coordinate, it is in this coordinate that we must also reduce the number of collocation points, $N^{\Phi}(\xi,\epsilon,\Omega,j)$. This is done by taking the points from the smallest region of space for which the potential and the wave functions are mapped onto the entire configuration space by successive symmetry operations. For Ar–H_2O, this region is $0 \le \phi \le \pi/2$. Note that it is inclusive of the end points.

TABLE II: The Form of the Points Used in This Application of the Collocation Method to Ar–H_2O

In the Radial Coordinate

i' is taken to range from 1 to N^R

$R_{i'} = R_i$, the center of the Gaussian, $\chi_i(R)$

In the θ Coordinate

j' is taken to range from 1 to N^{θ}

$\theta_{\xi'\epsilon'\Omega'j'}$ = the j'th Gauss–Legendre point from a set of Gauss–Legendre points of order N^{θ}

In the ϕ Coordinate

k' is taken to range from 1 to N^{Φ}, and k_{max} is the largest value of k to be included in any subblock of the calculation; $k_{max} = j$ when j is less than k_{max}; L is the largest value of k included in the subblock in question

Para Levels			
$\xi = 0$	k_{max} = even	$N^{\Phi} = (k_{max}+2)/2$	$\phi_{\xi'\epsilon'\Omega'j'k'} = 0$; $L = 0$ $\phi_{\xi'\epsilon'\Omega'j'k'} = (k'-1)\pi/L$
$\xi = 0$	k_{max} = odd	$N^{\Phi} = (k_{max}+1)/2$	$\phi_{\xi'\epsilon'\Omega'j'k'}$ as above
$\xi = 1$	k_{max} = even	$N^{\Phi} = (k_{max})/2$	$\phi_{\xi'\epsilon'\Omega'j'k'} = (2k'-1)\pi/2L$
$\xi = 1$	k_{max} = odd	$N^{\Phi} = (k_{max}-1)/2$	$\phi_{\xi'\epsilon'\Omega'j'k'}$ as above
Ortho Levels			
$\xi = 0$	k_{max} = even	$N^{\Phi} = (k_{max})/2$	$\phi_{\xi'\epsilon'\Omega'j'k'} = (2k'-1)\pi/2L$
$\xi = 0$	k_{max} = odd	$N^{\Phi} = (k_{max}+1)/2$	$\phi_{\xi'\epsilon'\Omega'j'k'}$ as above
$\xi = 1$	k_{max} = even	$N^{\Phi} = (k_{max})/2$	$\phi_{\xi'\epsilon'\Omega'j'k'} = (k'-1)\pi/L$
$\xi = 1$	k_{max} = odd	$N^{\Phi} = (k_{max}+1)/2$	$\phi_{\xi'\epsilon'\Omega'j'k'}$ as above

The convergence properties of the collocation method depend on the choice of both basis set and collocation points. The latter dependence is analogous to the dependence of Gaussian quadrature on the choice of grid points. No general method has been established for choosing such points, although optimal choices for some particular classes of functions are discussed by Peet and Yang in ref 17. For the calculation of the energies of Ar–H_2O using the Hamiltonian described above and the AW1 IPS, we observe convergence which is nearly identical with the atom–diatom results of Peet and Yang in the R and θ coordinates.[18,19] We find that on the interval R = 3–7 Å, with N^R = 30, and points taken at the centers of the Gaussians, the eigenvalues that are bound by at least 50 cm^{-1} are converged to 10^{-3} cm^{-1}. Eight functions in the θ coordinate, where we take the points to be Gauss–Legendre points of order 8, are required for similar convergence. The potential is 2-fold symmetric in ϕ, and fewer functions/points are therefore required in this coordinate. We have been able to converge the angular basis using only functions that have $k \le 6$ (3 or 4 functions and points in the ϕ coordinate included in each subblock).

Before completing our discussion of the convergence of the collocation procedure described, we elaborate on the choice of the number and position of the points in the ϕ coordinate. The number of points $N^{\Phi}(\xi,\epsilon,\Omega,j)$, for each of the four subblocks is approximately $k_{max}/2$, where k_{max} is the largest value of k included in the basis set for any of the subblocks (unless k_{max} is greater than j, in which case $k_{max} = j$). $N^{\Phi}(\xi,\epsilon,\Omega,j)$ is defined more completely in Table II. We take the points $\phi(\xi,\epsilon,\Omega,j)$ to be placed at the extrema of the highest order ϕ component of the wave function. The points are given by $(2k'-1)\pi/(2L)$ for the para, $\xi = 1$ functions and the ortho, $\xi = 0$ functions, and by $(k'-1)\pi/L$ for the para, $\xi = 0$ functions and the ortho, $\xi = 1$ functions. Here k' ranges from 1 to N^{Φ} and L is equal to the largest value of k included in that subblock. For values of $k_{max} \ge 5$, these points give convergence of Ar–H_2O energies that are equivalent to that realized with any other set which we have tried. For $k_{max} = 4$, which includes only two functions in ϕ in the ortho subblocks, we find more rapid convergence of the energies of the first few states in each ortho subblock using the points that are evenly spaced $(\pi/2;\ \pi/4,\ \pi/2)$ for $\xi = 0$ and $N^{\Phi}(\xi,\epsilon,\Omega,j) = 1;\ 2$, respectively, and $(0;\ 0,\pi/4)$ for $\xi = 1$, $N^{\Phi}(\xi,\epsilon,\Omega,j) = 1;\ 2$. We have no rationale for the improved performance of the calculation using these

particular points. The use of evenly spaced points with larger basis sets yields no improvement over the choice of the extrema of the functions as the points. Also, use of evenly spaced points for either of the para subblocks gives very slow convergence.

If the points described above are used, a basis set size for $J = 0$ of about 550 (slightly less than $N^R \times N^\theta \times N^\phi$, $(30 \times 8 \times 3)$, since not all functions in the ϕ coordinate are available for each j) is required for convergence to 0.001 cm^{-1}. Since the matrix size scales as $(2J + 1)$ this formulation rapidly exceeds available computer memory. For the purposes of iteratively fitting a potential, at least at this stage, it is satisfactory to concentrate on low J levels and we have not actively pursued methods of basis set contraction appropriate for high J. In the present work, we are also able to focus on the lowest levels of each symmetry (Γ), since only these have been accessed spectroscopically. Peet and Yang[19] found that using a contracted radial basis gave equivalent convergence with roughly half the functions required as when using uncontracted distributed Gaussians. Their method involved variational solution of a model one-dimensional problem to generate the contracted eigenvectors, followed by choosing points by the method of Harris, Engerholm, and Gwinn.[33] We have investigated a much simpler scheme for reducing the number of radial functions used, viz, reducing the interval over which they are distributed. We find convergence to 0.02 cm^{-1} for the energies of the levels of interest in the present least-squares fits with 11 radial functions distributed evenly between 3.05 and 4.65 Å. This radial basis is comparable in size and convergence properties for strongly bound levels to the contracted basis of Peet and Yang, although they are able to converge high-lying states to greater accuracy. The energies of the bound $J = 0$ and 1 levels of Ar–H_2O, calculated on the AW1 IPS described below, are given in Table III. All levels bound by more than 50 cm^{-1} are listed. These eigenvalues are converged to 0.01 cm^{-1} or better with a radial basis of $N^R = 15$, on the interval 3.0–5.0 Å, and an angular basis defined by $N^\theta = 7$ and $k_{max} = 5$. This basis is slightly larger than that used in our least-squares fits.

To summarize, we have described an extension of the collocation method that is capable of accurately evaluating the eigenvalues of a three-dimensional Hamiltonian with no dynamical approximations. The method is straightforward to apply to any atom–molecule system, and the eigenvalues are obtained sufficiently rapidly that the collocation subroutine may be placed within a least-squares loop and the difference between the calculated eigenvalues and measured experimental eigenvalues used to iteratively refine a model intermolecular potential.

III. The Intermolecular Potential Surface

The intermolecular potential energy surface for argon interacting with H_2O fixed at its ground-state geometry is evaluated in the body-fixed coordinate system described earlier. We take the z' axis of the monomer to be the C_{2v} axis and make the associations $a \rightarrow x'$ and $c \rightarrow y'$. The potential is expanded as a sum of terms that respectively represent an exponential repulsive wall, electrostatic induction, and dispersion:

$$V(R,\theta,\phi) = A(\theta,\phi)e^{-\beta R} + V_{induction}(R,\theta,\phi) - \sum_{n=6}^{8} C_n(\theta,\phi)\, D_n(R) R^{-n} \quad (9)$$

This form of the potential is constrained to have the theoretically correct form at long range while retaining sufficient flexibility to model the regions at short and intermediate range. Similar formulations have been used successfully by Hutson[2,4] and Leroy and Hutson[1] in fits of spectroscopic data for the rare gas–hydrogen halide and Rg–H_2 complexes. We have derived the form of the induction and dispersion contributions for an atom interacting with a molecule of C_{2v} symmetry from the generalized formulas for

(33) Harris, D. O.; Engerholm, G. G.; Gwinn, W. D. *J. Chem. Phys.* **1965**, 43, 1515.

TABLE III: Energy Levels (cm^{-1}) of the $J = 0$ and 1 States Calculated on the AW1 Potential[a]

	$J = 0$	
	A_1	A_2
1	−135.5428	none
2	−105.2739	
3	−95.3151	
4	−75.6432	
5	−70.7231	
6	−62.1225	
	$J = 1$	
	A_2	A_1
1	−135.3436	−98.3896
2	−105.0845	−68.9655
3	−98.4020	−63.2429
4	−95.1084	
5	−75.4661	
6	−70.6363	
7	−68.8575	
8	−63.2930	
9	−61.8895	
	$J = 0$	
	B_1	B_2
1	−82.5451	−118.7620
2	−50.5773	−84.7540
3		−60.9784
4		−54.2509
	$J = 1$	
	B_2	B_1
1	−107.1366	−118.5677
2	−97.5146	−107.1297
3	−82.3431	−97.5097
4	−74.6426	−84.5719
5	−63.7006	−74.6360
6	−56.9862	−63.6969
7	−50.3895	−60.8348
8		−56.9360
9		−54.0775

[a] These energies were calculated with a basis set defined by $N^R = 15$, $N^\theta = 7$, and $k_{max} = 5$, using a radial interval of 3.0–5.0 Å.

the interaction of any two species of arbitrary symmetry given by Buckingham:[34]

$$V_{induction}(R,\theta,\phi) = -\alpha\mu_z^2[1 + P_2(\cos(\theta))]R^{-6} - 2\alpha\mu_z(\Theta_{xx} - \Theta_{yy}) \sin^2(\theta) \cos(\theta) \times \cos(2\phi)R^{-7} - 4\alpha\mu_z[\Theta_{zz} - \tfrac{1}{2}(\Theta_{xx} + \Theta_{yy})] \cos^3(\theta)R^{-7} \quad (10)$$

and

$$C_6(\theta,\phi) = C_6\left\{1 + \left\{\left[\alpha_{zz} - \frac{1}{2}(\alpha_{xx} + \alpha_{yy})\right]/3\bar{\alpha}\right\}\frac{1}{2}(3\cos^2\theta - 1) + \{(\alpha_{xx} - \alpha_{yy})/3\bar{\alpha}\}\frac{3}{4}\sin^2(\theta)\cos(2\phi)\right\}$$

and

$$C_7(\theta,\phi) = C_6\{\{[6A_{xzx} + 6A_{yzy}]/3\bar{\alpha}\}\cos(\theta) + \{[6A_{zzz} - 4A_{xzx} - 4A_{yzy}]/3\bar{\alpha}\}\cos^3(\theta) + \{[-2A_{zzz} - 4A_{zyy} - 4A_{xzx} + 4A_{yzy}]/3\bar{\alpha}\}\sin^2(\theta)\cos(\theta)\cos(2\phi)\} \quad (11)$$

The molecular constants of H_2O, which are accurately known from experiment, have been fixed at the values given in Table IV. The rotational constants,[35] permanent moments (μ,[36] Θ[37]), and the dipole polarizabilities (α[38]) of water are experimental values. The

(34) Buckingham, A. D. *Adv. Chem. Phys.* **1967**, *12*, 107.
(35) Johns, J. W. *J. Opt. Soc. Am. B. Opt. Phys.* **1985**, *2*, 1340.
(36) Dyke, T. R.; Muenter, J. S. *J. Chem. Phys.* **1976**, *59*, 3125.
(37) Verhoeven, J.; Dymanus, A. *J. Chem. Phys.* **1970**, *52*, 3222.

TABLE IV: Molecular and Atomic Constants for H_2O and Argon

A = 27.8806 cm^{-1}	ref 35
B = 9.2778 cm^{-1}	
C = 14.5216 cm^{-1}	
μ_z = 0.7298 e a_0^2	ref 36
Θ_{xx} = 1.96 e a_0^3	ref 37
Θ_{yy} = −1.86 e a_0^3	
Θ_{zz} = −0.097 e a_0^3	
α_{xx} = 10.311 a_0^3	ref 38
α_{yy} = 9.549 a_0^3	
α_{zz} = 9.907 a_0^3	
α = 9.922 a_0^3	
A_{zzz} = 2.194 a_0^4	ref 40
A_{zyy} = −4.070 a_0^4	
A_{xzx} = 6.742 a_0^4	
A_{yzy} = 1.786 a_0^4	
polarizability of argon α = 11.096 a_0^3	ref 39
pseudodiatomic reduced mass μ = 12.419126 amu	
isotropic dispersion const for Ar–H_2O C_6 = 55.7 $E_h(a_0)^6$	estimate, see text

dipole polarizability of argon is also fixed at the experimental value.[39] The dipole–quadrupole polarizabilities (A_{ijk}) for H_2O are the result of a CI-SCF calculation by John, Bacskay, and Hush.[40] These appear to be the most accurate calculations available for the polarizabilities of H_2O. Those constants which are not available, namely $A(\theta,\phi)$, $C_8(\theta,\phi)$, and β, were determined by a least-squares fit to the far-infrared VRT data. The data were not capable of accurately determining the value of C_6. We have accordingly fixed it at C_6 = 55.7 hartree a_0^6. This value is estimated from the usual combining rule; it is the geometric mean of the C_6 constants for Ar_2 (C_6 = 68.5 hartree a_0^6)[41] and for $(H_2O)_2$ (C_6 = 48.37 hartree a_0^6).[42] The functions $D_n(R)$ are used to damp the dispersion energy at short range. We use the damping functions proposed by Tang and Toennies[43]

$$D_n(R) = 1 - e^{-\beta R}\sum_{m=0}^{n}\frac{(\beta R)^m}{m!} \tag{12}$$

The constant β in this function is identical with that used in the exponential form of the repulsive wall.

In order to implement least-squares fits, it is convenient to develop a simple and numerically stable parametrization of the above potential. We have chosen a simple variant of the parametrization used by Hutson in his determination of the Ar–HCl IPS.[2] We expand the well depth and the position of the radial minimum in symmetry-adapted renormalized spherical harmonics:

$$\epsilon(\theta,\phi) = \sum_{\lambda\mu}\epsilon_{\lambda\mu}C_{\lambda\mu}(\theta,\phi)$$

$$R^m(\theta,\phi) = \sum_{\lambda\mu}R^m{}_{\lambda\mu}C_{\lambda\mu}(\theta,\phi)$$

$$C_{\lambda\mu}(\theta,\phi) = \left[\left(\frac{4\pi}{2\lambda+1}\right)^{1/2}Y_{\lambda,\mu}(\theta,\phi) + (-1)^{\mu}\left(\frac{4\pi}{2\lambda+1}\right)^{1/2}Y_{\lambda,-\mu}(\theta,\phi)\right](1+\delta_{0\mu})^{-1} \tag{13}$$

The symmetry-adapted renormalized spherical harmonics $C_{\lambda\mu}$ are used, since they have the same normalization as the Legendre polynomials. The coefficients are thus directly comparable to those of atom–diatom systems, for which a Legendre parametrization has been utilized.[26] The coefficients $\epsilon_{\lambda\mu}$, $R^m{}_{\lambda\mu}$, and β are the quantities that are actually varied during the course of the least-squares fits. We use the following two relations to derive the relationship of the unknowns $A(\theta,\phi)$ and $C_8(\theta,\phi)$ to the parameters $\epsilon_{\lambda\mu}$, and $r^m{}_{\lambda\mu}$: (1) $V(R_m(\theta,\phi);\theta,\phi) = -\epsilon(\theta,\phi)$ and (2) $V'(R_m(\theta,\phi);\theta,\phi) = 0$, where the prime indicates the first derivative with respect to R. Formulas for deriving $A(\theta,\phi)$ and $C_8(\theta,\phi)$ are analogous to those given by Hutson:[1,2]

$$V_{\text{fix}}(R,\theta,\phi) = V_{\text{induction}}(R,\theta,\phi) - C_6(\theta,\phi)\,D_6(R)R^{-6} - C_7(\theta,\phi)\,D_7(R)R^{-7}$$

$$C_8(\theta,\phi) = [\{\beta[\epsilon(\theta,\phi) + V_{\text{fix}}(R_m(\theta,\phi),\theta,\phi)] + V'_{\text{fix}}(R_m(\theta,\phi),\theta,\phi)\}R_m^8(\theta,\phi)][D'_8(R_m(\theta,\phi) - D_8(R_m(\theta,\phi)[8/R_m(\theta,\phi) - \beta]]^{-1}$$

$$A(\theta,\phi) = [C_8(\theta,\phi)D_8(R_m(\theta,\phi))R_m(\theta,\phi)^{-8} - \epsilon(\theta,\phi) + V_{\text{fix}}(R_m(\theta,\phi),\theta,\phi)]e^{\beta R_m(\theta,\phi)} \tag{14}$$

IV. The AW1 Potential

We have used the collocation method to calculate intermolecular vibrational frequencies and rotational term values for Ar–H_2O, using the model potential surface described in the preceding section. The IPS was refined by a nonlinear least-squares fit to the experimental values for these properties, which were determined from tunable far-infrared laser spectroscopy. To date, seven different intermolecular vibrational levels of Ar–H_2O have been sampled through the measurement of four vibration–rotation bands of Ar–H_2O. Two bands were assigned as internal rotor transitions (in a rigid molecule these correspond to bending vibrations), and two were assigned to the intermolecular stretch. Figure 6 graphically summarizes the spectroscopically measured energy differences and shows the postions of all other vibrational levels bound by more than 48 cm^{-1}. The energies are relative to the lowest dissociation limit, as calculated from the optimized IPS (hereafter called AW1). The intermolecular vibrational energy levels are labeled by the projection of the vibrational angular momentum (Ω), on the cluster a axis, by the monomer rotational state to which it correlates in the free rotor limit (j_{kakc}), and by the number of quanta in the intermolecular stretching mode (n). For simplicity we often omit reference to n when n = 0. Thus, n = 0, $\Pi(1_{10})$ and $\Pi(1_{10})$ refer to the same state.

In this initial effort we have required the potential energy surface to reproduce only data associated with two total angular momentum states: J = 0 and J = 1. These data are summarized in Table V. Calculations within the least-squares loop were performed with a basis of N^R = 11 on the interval 3.05–4.65 Å,

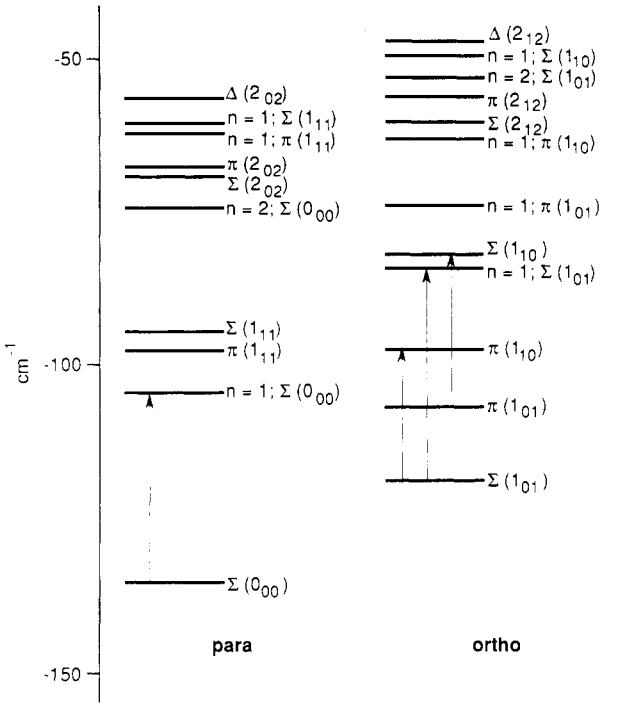

Figure 6. An energy level diagram for Ar–H_2O derived from the AW1 potential, the para and ortho levels are shown in separate columns for the sake of clarity.

(38) Murphy, W. F. *J. Chem. Phys.* **1977**, *67*, 5877.
(39) Tang, K. T.; Norbeck, J. M.; Certain, P. R. *J. Chem. Phys.* **1976**, *64*, 3063. Reinsch, E. A.; Meyer, W. *Phys. Rev. A* **1976**, *14*, 915.
(40) John, I. G.; Bacskay, G. B.; Hush, N. S. *Chem. Phys.* **1980**, *51*, 49.
(41) Fowler, P. W.; Hutson, J. M. *Surf. Sci.* **1986**, *165*, 289.
(42) Buckingham, A. D.; Fowler, P. W.; Hutson, J. M. *Chem. Rev.* **1988**, *88*, 963.
(43) Tang, K. T.; Toennies, J. P. *J. Chem. Phys.* **1984**, *80*, 3726.

TABLE V: Vibrational Transitions and Rotational Term Values (MHz) Included in the Least-Squares Fits To Determine the AW1 Potential[a]

Rotational Term Values

v	$J \leftarrow J$	rovibrnl sym	exptl	calcd	residuals	unc.
$\Sigma(0_{00})$	$1 \leftarrow 0$	$A_2 \leftarrow A_1$	5975.8	5970.4	5.4	2.0
n = u, $\Sigma(0_{00})$	$1 \leftarrow 0$	$A_2 \leftarrow A_1$	5676.5	5678.6	−2.1	2.0
$\Sigma(1_{01})$	$1 \leftarrow 0$	$B_1 \leftarrow B_2$	5824.2	5828.2	−4.0	2.0
n = l, $\Sigma(1_{01})$	$1 \leftarrow 0$	$B_1 \leftarrow B_2$	5461.6	5460.0	1.6	2.0
$\Sigma(1_{10})$	$1 \leftarrow 0$	$B_2 \leftarrow B_1$	6052.8	6053.9	−1.1	2.0
$\Pi(1_{01})$	$1 \leftarrow 1$	$B_2 \leftarrow B_1$	205.1	205.1	0.0	0.3
$\Pi(1_{10})$	$1 \leftarrow 1$	$B_1 \leftarrow B_2$	146.8	146.7	0.1	0.3

Rovibrational Transitions

$v \leftarrow v$	$J \leftarrow J$	rovibrnl sym	exptl	calcd	residuals	unc.
n = l, $\Sigma(0_{00}) \leftarrow \Sigma(0_{00})$	$1 \leftarrow 0$	$A_2 \leftarrow A_1$	912998.4	913254	−255	500.0
n = l, $\Sigma(1_{01}) \leftarrow \Sigma(1_{01})$	$0 \leftarrow 1$	$B_1 \leftarrow B_2$	1013415.2	1013250	165	500.0
$\Pi(1_{10}) \leftarrow \Sigma(1_{01})$	$1 \leftarrow 0$	$B_1 \leftarrow B_2$	637466.9	637252	214	500.0
$\Sigma(1_{10}) \leftarrow \Pi(1_{01})$	$0 \leftarrow 1$	$B_2 \leftarrow B_1$	738047.3	737878	169	500.0

[a] Experimental values are derived from the constants of ref 7.

TABLE VI: Constants Determined for the AW1 Potential[a]

β = 2.501 (32) Å^{-1}	R^m_{00} = 3.6339 (13) Å
ϵ_{00} = 153.3 (22) cm^{-1}	R^m_{10} = 0.1005 (10) Å
ϵ_{10} = 1.90 (24) cm^{-1}	R^m_{20} = 0.0128 (36) Å
ϵ_{20} = 4.518 (72) cm^{-1}	R^m_{22} = −0.0342 (17) Å
ϵ_{22} = 19.301 (54) cm^{-1}	DSE = 1.14

Correlation Matrix

β									
ϵ_{00}	−0.98								
ϵ_{10}	0.13	−0.09							
ϵ_{20}	−0.04	0.01	−0.16						
ϵ_{22}	0.51	−0.55	−0.15	0.34					
R^m_{00}	−0.84	0.85	−0.12	0.03	−0.53				
R^m_{10}	0.22	−0.12	0.28	−0.38	−0.17	−0.18			
R^m_{20}	−0.23	0.27	0.14	0.05	−0.17	0.41	−0.17		
R^m_{22}	−0.37	0.37	−0.06	−0.01	−0.11	0.16	0.06	0.26	
	β	ϵ_{00}	ϵ_{10}	ϵ_{20}	ϵ_{22}	R^m_{00}	R^m_{10}	R^m_{20}	R^m_{22}

[a] The errors shown are 2σ uncertainties.

$N^\theta = 6$, and $k_{max} = 4$. This gives a matrix size of about 120 for the $J = 0$ subblocks and about 360 for the $J = 1$ subblocks. With this basis, vibrational frequencies used in the fit are converged to 0.02 cm^{-1} and $J = 1 \leftarrow 0$ rotational term values to about 2.0 MHz. Each call to the energy level subroutine required 120 s of CPU time and a single iteration of the least-squares loop for nine parameters requires about 18 min of CPU time on the Berkeley Cray-XMP. Nine parameters were allowed to vary in a simultaneous weighted least-squares fit to 11 data points. The data were weighted by the inverse square of our estimate of the uncertainty in the calculated energy differences. The residuals from the fit are shown in Table V and the potential constants determined are collected in Table VI. We note that the correlations among the parameters are quite low.

The resulting potential has a minimum at $\theta = 85.7°$ and $\phi = 0°$ at $R = 3.598$ Å with a well depth of 174.7 cm^{-1}. In the body-fixed coordinate system, $\phi = 0$ corresponds to planar geometries. At $\theta = 0°$ the argon bisects the two hydrogens along the C_{2v} axis, while at $\theta = 180°$ the argon is in the opposing orientation, nearest the oxygen atom. The equilibrium geometry is therefore a nearly perpendicular alignment of the water C_{2v} axis to the a inertial axis of the cluster.

Figures 1–4 show several cuts through the AW1 PES. These show that the anisotropy in θ is small, especially in the region near the minimum. For ϕ closer to 90°, the anisotropy in θ is somewhat larger with a maximum in the barrier to internal rotation appearing at $\theta = 90°$, $\phi = 90°$, which is 47 cm^{-1} above the absolute minimum. The relatively small anisotropy in the IPS for Ar–H_2O is discussed by Hutson,[26] who argues that it results because the dipolar and quadrupolar contributions to the induction forces do not reinforce each other. Anisotropy in the dispersion and repulsive forces is expected to be similar to that in the induction forces. At R_{min}, the IPS varies by 20 cm^{-1} for rotation in the plane of the H_2O, with barriers at both $\theta = 0°$ and $\theta = 180°$. Substantial variation in the anisotropy as a function of radial position (angular–radial coupling) is clearly evidenced. In the plane of the H_2O monomer, the repulsive wall rises more sharply with larger R at $\theta = 0°$ than it does at $\theta = 180°$; the minimum energy path for an argon rotating about the center of mass of H_2O is not at a constant radius. This is not unexpected, since the hydrogen atoms extend much further from the center of mass of the H_2O subunit than does the electron distribution about the oxygen atom. Also, as can be seen in Figure 3, at increasing intermolecular separations the magnitude of the anisotropy decreases and the positions of the angular minima and maxima change. At $R = 4.0$ Å, the position of the minimum shifts toward smaller θ, appearing in the vicinity of $\theta = 40°$, $\phi = 0°$, while the maximum shifts to larger θ, appearing at $\theta = 110°$, $\phi = 90°$. Excited stretching states can thus be expected to sample a different subspace of the angular degrees of freedom in the IPS than do $n = 0$ levels.

The parameters which determine the form of the AW1 potential are accurately determined with uncertainties of 25% or less at the 2σ level, and with small correlations between most of the parameters. The only large correlations are between β and the isotropic well depth, ϵ_{00} (0.98), and between these two parameters and r^m_{00} (−0.84, and 0.85). The quality of the fit, as measured by the dimensionless standard error,[1] is quite good with the DSE = 1.14. Measurement of additional vibration–rotation bands and inclusion of term values involving higher J levels can be used in the future to develop a still more accurate and independent set of parameters. More importantly, with the inclusion of additional data it will be possible to fit more parameters. In particular, it will be possible to investigate whether the ab initio values for the dipole–quadrupole polarizabilities and the crude estimate of the isotropic dispersion constant used in the AW1 potential are sufficiently accurate. It will also be of interest to investigate the convergence of the spherical harmonic representation of the potential. The largest anisotropic term in the well depth expansion is also the term of highest order, which may indicate that this expansion is converging slowly. In contrast, the expansion of the position of the radial minimum appears to be rapidly converging. Another consideration is the degree of flexibility in the ϕ coordinate; only two parameters included in the AW1 parametrization allow flexibility in this coordinate, ϵ_{22} and r^m_{22}. Additional flexibility may be necessary in a more accurate potential.

To aid in the search for and identification of additional bands of Ar–H_2O, we summarize in Table VII the frequencies of vibrational transitions and rotational term values (calculated with a basis set of $N^R = 11$, $N^\theta = 6$, and $N^\phi = 4$, on the radial interval 3.05–4.65 Å) for a number of the low-lying vibrational levels of Ar–H_2O. With the exception of the 1_{11} states discussed below, the frequencies predicted for the bending transitions are in the same wavenumber range as those predicted by Hutson on the $V_{10} = 0$ potential. In contrast, the rotational term values would be difficult to predict with such approximate methods. The effects of Coriolis mixing is pronounced, leading to rotational spacings

TABLE VII: Predicted Vibrational Frequencies and Rotational Term Values for Some of the States of Ar–H_2O[a] (MHz)

		calcd	exptl
	Rotational Term Values		
$J = 1 \leftarrow 0$			
$\Sigma(0_{00})$	$A_2 \leftarrow A_1$	5970.4	5975.8
$\Sigma(1_{11})$	$A_2 \leftarrow A_1$	6186.2	
$\Sigma(2_{02})$	$A_2 \leftarrow A_1$	2088.3	
$\Sigma(1_{01})$	$B_1 \leftarrow B_2$	5828.2	5824.2
$\Sigma(1_{10})$	$B_2 \leftarrow B_1$	6053.9	6052.8
$\Sigma(2_{12})$	$B_1 \leftarrow B_2$	4262.5	
$n = 1$, $\Sigma(0_{00})$	$A_2 \leftarrow A_1$	5678.6	5676.5
$n = 1$, $\Sigma(1_{01})$	$B_1 \leftarrow B_2$	5460.0	5461.6
$J = 1 \leftarrow 1$			
$\Pi(1_{11})$	$A_1 \leftarrow A_2$	362.1	
$\Pi(2_{02})$	$A_1 \leftarrow A_2$	-3749.3	
$\Pi(1_{01})$	$B_1 \leftarrow B_2$	205.1	205.1
$\Pi(1_{10})$	$B_1 \leftarrow B_2$	146.7	146.8
$\Pi(2_{12})$	$B_1 \leftarrow B_2$	1559.3	
$n = 1$, $\Pi(1_{01})$	$B_1 \leftarrow B_2$	196.0	
$J = 2 \leftarrow 1$			
$\Sigma(0_{00})$	$A_1 \leftarrow A_2$	11938.3	11949.5
$\Sigma(1_{11})$	$A_1 \leftarrow A_2$	12369.1	
$\Pi(1_{11})$	$A_1 \leftarrow A_2$	11254.0	
$\Sigma(2_{02})$	$A_1 \leftarrow A_2$	5568.3	
$\Pi(2_{02})$	$A_1 \leftarrow A_2$	17673.4	
$\Sigma(1_{01})$	$B_2 \leftarrow B_1$	11654.7	11647.0
$\Pi(1_{01})$	$B_1 \leftarrow B_2$	11806.1	11804.8
$\Sigma(1_{10})$	$B_1 \leftarrow B_2$	12105.1	12103.0
$\Pi(1_{10})$	$B_1 \leftarrow B_2$	11775.3	11855.5
$\Sigma(2_{12})$	$B_2 \leftarrow B_1$	8643.4	
$\Pi(2_{12})$	$B_1 \leftarrow B_2$	11247.6	
$n = 1$, $\Sigma(0_{00})$	$A_1 \leftarrow A_2$	11355.9	11332.3
$n = 1$, $\Sigma(1_{01})$	$B_2 \leftarrow B_1$	10918.4	10920.5
$n = 1$, $\Pi(1_{01})$	$B_1 \leftarrow B_2$	11101.1	
$J = 2 \leftarrow 2$			
$\Pi(1_{11})$	$A_2 \leftarrow A_1$	1086.8	
$\Pi(2_{02})$	$A_2 \leftarrow A_1$	-9849.7	
$\Delta(2_{02})$	$A_2 \leftarrow A_1$	-6.2	
$\Pi(1_{01})$	$B_2 \leftarrow B_1$	614.7	614.6
$\Pi(1_{10})$	$B_2 \leftarrow B_1$	439.7	440.6
$\Pi(2_{12})$	$B_2 \leftarrow B_1$	4541.6	
$\Delta(2_{12})$	$B_2 \leftarrow B_1$	2.9	
$n = 1$, $\Pi(1_{01})$	$B_2 \leftarrow B_1$	587.1	
	Vibrational Transitions		
$\Sigma(1_{11}) \leftarrow \Sigma(0_{00})$	$J = 1 \leftarrow 0$, $A_2 \leftarrow A_1$	1212322.0	
$\Pi(1_{11}) \leftarrow \Sigma(0_{00})$	$J = 1 \leftarrow 0$, $A_2 \leftarrow A_1$	1112431.0	
$n = 1$, $\Sigma(1_{11}) \leftarrow \Sigma(0_{00})$	$J = 1 \leftarrow 0$, $A_2 \leftarrow A_1$	913254.5	912998.4
$\Sigma(2_{02}) \leftarrow \Sigma(0_{00})$	$J = 1 \leftarrow 0$, $A_2 \leftarrow A_1$	1950994.4	
$\Pi(2_{02}) \leftarrow \Sigma(0_{00})$	$J = 1 \leftarrow 0$, $A_2 \leftarrow A_1$	1997882.4	
$\Pi(1_{01}) \leftarrow \Sigma(1_{01})$	$J = 1 \leftarrow 0$, $B_1 \leftarrow B_2$	349559.0	
$\Pi(1_{10}) \leftarrow \Sigma(1_{01})$	$J = 1 \leftarrow 0$, $B_1 \leftarrow B_2$	637252.5	637466.9
$n = 1$, $\Sigma(1_{01}) \leftarrow \Sigma(1_{01})$	$J = 1 \leftarrow 0$, $B_1 \leftarrow B_2$	1024537.9	1024701.0
$\Sigma(2_{12}) \leftarrow \Sigma(1_{01})$	$J = 1 \leftarrow 0$, $B_1 \leftarrow B_2$	1739568.5	
$\Pi(2_{12}) \leftarrow \Sigma(1_{01})$	$J = 1 \leftarrow 0$, $B_1 \leftarrow B_2$	1853301.5	
$\Pi(1_{10}) \leftarrow \Pi(1_{01})$	$J = 1 \leftarrow 1$, $B_1 \leftarrow B_2$	287898.6	
$\Sigma(1_{10}) \leftarrow \Pi(1_{01})$	$J = 0 \leftarrow 1$, $B_1 \leftarrow B_2$	737878.2	738047.3
$n = 1$, $\Pi(1_{01}) \leftarrow \Pi(1_{01})$	$J = 1 \leftarrow 1$, $B_1 \leftarrow B_2$	974370.1	
$\Sigma(2_{12}) \leftarrow \Pi(1_{01})$	$J = 0 \leftarrow 1$, $B_1 \leftarrow B_2$	1385952.1	
$\Pi(2_{12}) \leftarrow \Pi(1_{01})$	$J = 1 \leftarrow 1$, $B_1 \leftarrow B_2$	1503947.6	
$\Delta(2_{12}) \leftarrow \Pi(1_{01})$	$J = 2 \leftarrow 1$, $B_1 \leftarrow B_2$	1760662.2	

[a] They were calculated with a basis set of $N^R = 11$, $N^\theta = 6$, and $k_{max} = 4$, on a radial interval 3.05–4.65 Å.

which deviate significantly from the values which would be predicted based on structural parameters alone.

Also listed in Table VII are experimental values for the vibrational frequencies and rotational term values calculated from the constants of ref 7. None of the rotational term values involving $J = 2$ were included in the least-squares fits because of the increased computational effort required. The largest differences between the experimental values and those calculated on the AW1 surface are for the lowest rotational term values ($J = 2 \leftarrow 1$) of the two Π states which have been observed spectroscopically. The difference is of the order 0.01 cm^{-1}. In future work, when a larger experimental data set is available, these term values will be included in a refinement of the AW1 IPS.

V. Discussion

The AW1 potential is in excellent agreement with previous approximate studies of the Ar–H_2O IPS. Hutson calculated[26] a range of parameters V_{10}, V_{20}, and V_{22} within the "reversed adiabatic" approximation which are capable of reproducing the measured bending frequencies reported in ref 6. Our Coriolis analysis of this data, given in ref 7, suggested that the most likely potential, of the several considered by Hutson, was that with $V_{10} = 0$, $V_{20} = 5.14$, and $V_{22} = 17.58$ in units of cm^{-1}. The values determined from the full three-dimensional analysis in the present work are $\epsilon_{10} = 1.90$ (24), $\epsilon_{20} = 4.518$ (72), and $\epsilon_{22} = 19.301$ (54). These parameters produce a potential, shown in Figure 2, with the same qualitative appearance as Hutson's $V_{10} = 0$ potential shown in Figure 4 of ref 26. Although similar in notation and form, the well-depth parameters which describe AW1 IPS are not strictly comparable to those determined by Hutson within the "reversed adiabatic" approximation. The well-depth parameters of the AW1 IPS reflect both the anisotropy in the region of the potential minimum and the angular–radial coupling, which is specifically neglected in the reversed adiabatic approximation.

The close agreement with the parameters of the $V_{10} = 0$ potential of Hutson indicates that the reversed adiabatic approximation provides an accurate estimate of the relation between the anisotropy in the PES and measured bending frequencies for the Ar–H_2O complex. Such approximate relationships must be interpreted with care, however. Although Hutson's $V_{10} = 0$ potential reproduces the lowest ortho bending frequencies of Ar–H_2O, the first para bending levels are extremely sensitive to the degree of angular–radial coupling in the potential. On the $V_{10} = 0$ potential the $\Sigma(1_{11})$ state is about 1.0 cm^{-1} below the $\Pi(1_{11})$ state. The situation is reversed on the AW1 IPS with the $\Pi(1_{11})$ state about 3.0 cm^{-1} below the $\Sigma(1_{11})$ state. Calculations on several different model potentials indicate that the energies of these two vibrational levels are strongly affected by anisotropy in the position of the radial minimum (which is specified by the values of $R^m{}_{\lambda\mu}$). In addition, at values of the potential parameters where the states become nearly degenerate, the effects of Coriolis matrix elements are substantial, in some cases indicating $J = 1$, $\Sigma(1_{11})$ as being more strongly bound than $J = 0$, $\Sigma(1_{11})$. The sensitivity to the degree of angular–radial coupling of these two states may arise because of their near-degeneracy and/or because of the region of the potential which they sample. The latter seems more likely, since other near-degenerate states (e.g., Σ and $\Pi(2_{02})$) are not nearly as sensitive to the values of $R^m{}_{\lambda\mu}$. The $\Sigma(1_{11})$ level, which is most strongly affected by changes in the anisotropy of the position of the radial minimum, is a vibrational level with motion characterized by rotation about the b axis of H_2O with that axis perpendicular to the a axis of the cluster. This state thus samples both the absolute minimum of the potential at $\theta = 90°$, $\phi = 0°$ and the barrier to internal rotation at $\theta = 90°$, $\phi = 90°$. Small changes in the angular radial coupling might affect the relative energy of this state more than others because of the wide range of the potential it thus probes. By contrast, the $\Sigma(1_{01})$ level, which is not substantially shifted by such changes, samples the potential in the plane of the global minimum and thus experiences a smaller variation in the PES. Additional study is clearly required to be able to unambiguously identify those cases in which the reversed adiabatic approximation yields reliable results.

The dissociation energy of the AW1 potential ($D_e = 174.7$ cm^{-1}) is also in qualitative agreement with the value of $D_e = 153$ cm^{-1} estimated from the effective radial potential for the $\Sigma(1_{01})$ vibrational level, which we determined by fit to the measured rotational term values.[7] This was the deepest minimum among the three effective radial potentials that we determined and was presumed to reflect the minimum energy of the full anisotropic potential most closely. Much of the difference between the two dissociation energies can be attributed to zero-point energy in the bending coordinate, which is not present in the effective radial

IPS. The dissociation energy (D_e) of the $\Sigma(0_{00})$ ground state on its effective radial IPS was determined to be 126 cm^{-1}. This is of the same order as the D_0 of the AW1 potential surface, which is 135.6 cm^{-1}. The smaller difference between the two indicates that this level is not as strongly affected by the anisotropy in the three-dimensional IPS. The third effective radial potential determined was for the $\Sigma(1_{10})$ state. The binding energy of the state was D_e = 98 cm^{-1}. The difference between this value and that for the $\Sigma(1_{01})$ vibrational level is 55 cm^{-1}, which appears to be a reasonable estimate of the magnitude of the anisotropy in the IPS. As noted above, the maximum barrier to internal rotation is at $\theta = 90°$, $\phi = 90°$ 47 cm^{-1} above the global minimum. Finally, we note that the AW1 potential is in reasonable agreement with the well depth of several previous isotropic Lennard-Jones potentials determined from molecular beam scattering[27] (σ = 2.9 Å, ϵ = 125 cm^{-1}) and solubility measurements (σ = 3.44 Å, ϵ = 133 cm^{-1}).[28] No high-level ab initio calculations are available for this system. The calculations that have been performed[44,45] severely underestimate the well depth (75 cm^{-1}) and predict a global minimum at the $\theta = 0°$, $\phi = 0°$ in contrast to the experimental results presented here.

In conclusion, we have developed an application of the collocation method which extends this powerful new technique for calculating the bound-state energies and the wave functions of molecules with strongly coupled degrees of freedom to three-dimensional systems. The method is efficient and simple to implement. As a test of the method, we have incorporated it within a least-squares loop and used it to iteratively determine an accurate anisotropic potential for Ar–H_2O. It is our hope that this potential will be of use in investigations of the effects of anisotropic forces in condensed phases, and in particular, with regard to their contribution to the effects commonly referred to as the "hydrophobic interaction".

Improvements in the methodology outlined above for calculating the bound states of multidimensional systems should allow the IPS of dimers and trimer to be routinely determined from experimental measurements. The most important improvements will consist of improved basis functions, such as the Sturmian functions used by Choi and Light[23] for the radial coordinate in their study of Ar–HCl, improved basis set contraction schemes, and in the application of iterative methods to the solution of large generalized unsymmetrical eigenvalue problems. These last two have been discussed by Peet and Yang.[19,21] In the near future, such advances can be expected to allow significantly more complex systems to be addressed in the quest for a deeper understanding of the details of intermolecular forces.

Acknowledgment. We thank A. C. Peet and W. Yang for providing us with copies of their recent papers prior to publication. Calculations described in this work were performed on the Berkeley Cray-XMP. We are grateful to University of California at Berkeley for a generous grant of computer time to pursue this project. This work was supported by the Director, Office of Energy Research, Office of Basic Energy Sciences, Chemical Sciences Division of the U.S. Department of Energy, under contract No. DE-AC03-76SF00098.

Registry No. Ar, 7440-37-1; H_2O, 7332-18-5.

(44) Losonczy, M.; Moskowitz, J. W.; Stillinger, F. H. *J. Chem. Phys.* **1973**, *59*, 3264.
(45) Kolos, W.; Corongiu, G.; Clementi, E. *Int. J. Quantum Chem.* **1980**, *17*, 775.